Tellus
SERIES A
DYNAMIC
METEOROLOGY
AND OCEANOGRAPHY
PUBLISHED BY THE INTERNATIONAL METEOROLOGICAL INSTITUTE IN STOCKHOLM

Tellus (2011), 63A, 107–125
Printed in Singapore. All rights reserved

TELLUS

High-resolution regional simulation of last glacial maximum climate in Europe

By GUSTAV STRANDBERG[1]*, JENNY BRANDEFELT[2], ERIK KJELLSTRÖM[1] and BENJAMIN SMITH[3], [1]*Swedish Meteorological and Hydrological Institute, SE-60176 Norrköping, Sweden*; [2]*Department of Mechanics, Linné Flow Centre, KTH, SE-10044 Stockholm, Sweden*; [3]*Department of Earth and Ecosystem Sciences, Lund University, Geocentrum II, SE-22362 Lund, Sweden*

(Manuscript received 26 January 2010; in final form 6 September 2010)

ABSTRACT

A fully coupled atmosphere–ocean general circulation model is used to simulate climate conditions during the last glacial maximum (LGM). Forcing conditions include astronomical parameters, greenhouse gases, ice sheets and vegetation. A 50-yr period of the global simulation is dynamically downscaled to 50 km horizontal resolution over Europe with a regional climate model (RCM). A dynamic vegetation model is used to produce vegetation that is consistent with the climate simulated by the RCM. This vegetation is used in a final simulation with the RCM. The resulting climate is 5–10 °C colder than the recent past climate (representative of year 1990) over ice-free parts of Europe as an annual average; over the ice-sheet up to 40 °C colder in winter. The average model-proxy error is about the same for summer and winter, for pollen-based proxies. The RCM results are within (outside) the uncertainty limits for winter (summer). Sensitivity studies performed with the RCM indicate that the simulated climate is sensitive to changes in vegetation, whereas the location of the ice sheet only affects the climate around the ice sheet. The RCM-simulated interannual variability in near surface temperature is significantly larger at LGM than in the recent past climate.

1. Introduction

The last glacial maximum (LGM, ∼21 kyr BP) is characterized by the largest ice volume in the last glacial cycle (i.e. the last 100 000 yr) and very cold conditions. Climate models indicate that the annual global mean temperature (T_{globe}) was 1.85–9.17 °C lower than present (Kageyama et al., 2006; Braconnot et al., 2007). Proxy data are sparse for the LGM thus limiting the possibility to build global reconstructions from proxy data only. In a model ensemble constrained by proxy data, Schneider von Deimling et al. (2006) find that T_{globe} is 4–7 °C colder at LGM than in the pre-industrial climate. Regionally, differences were larger, for example at the ice sheets at high northern latitudes. Another consequence of the colder and also generally drier climate during LGM was that vegetation cover differed from present (e.g. Harrison and Prentice, 2003). The height of the ice sheets and the extent of different vegetation types and their respective influence on the LGM climate is uncertain. Proxy data have biases and may give a picture that is sometimes contradictory to and in conflict with climate models, because of uncertainties in the reconstructed climate and uncertainties in the chronology of the reconstructions (Kageyama et al., 2006). Three-dimensional reconstructions of both surface conditions and properties of the large-scale circulation are rare but attempts have been made utilising proxy data from several sources (e.g. Kuhlemann et al., 2008). In this study model results are compared with proxies for sea surface temperatures (SSTs) based on microfossils, temperature and precipitation based on pollen and temperature based on palaeo glaciers.

Coupled atmosphere–ocean general circulation models (AOGCMs) give a three-dimensionally consistent picture of the atmosphere and ocean irrespective of choice of time period and independent of proxy-based reconstructions of the climate (as long as those are not used to build the boundary conditions). AOGCMs have been shown to simulate many aspects of today's climate in a realistic way (Randall et al., 2007). Evaluation of AOGCMs under pre-instrumental conditions is more difficult because there are no instrumental observations and the amount of palaeoclimatic records are limited (Jansen et al., 2007). In spite of this, AOGCMs have been applied to and tested for periods such as the LGM in the Palaeoclimate Modelling Intercomparison Projects (PMIP1, e.g. Joussaume and Taylor, 1995 and PMIP2, Braconnot et al., 2007) showing that the models are able to simulate many of the major processes determining the LGM

*Corresponding author.
e-mail: gustav.strandberg@smhi.se
DOI: 10.1111/j.1600-0870.2010.00485.x

Table 1. High-resolution simulations of LGM climate for Europe

Author	Model	Resolution over Europe	Analysed time period (yr)	SST	Ice sheets
Pollard and Barron (2003)	RegCM2 nested in GENESIS GCM	60 km	6	Prescribed[a]	ICE-4G[b]
Jost et al. (2005)	LMDZ GCM	60 km[c]	10	Prescribed[a]	ICE-4G[b]
	CCSR	T106 ≈ 190 km	10	Prescribed[a]	ICE-4G[b]
	HadRM nested in HadAM3	0.44° ≈ 50 km	5	Prescribed[a]	ICE-4G[b]
This work	RCA3 nested in CCSM3	0.44° ≈ 50 km	50	From CCSM3	ICE-5G

[a]CLIMAP (1981).
[b]ICE-4G (Peltier, 1994).
[c]The model operates with a stretched grid. Sixty kilometres is the highest horizontal resolution in France.

climate state given appropriate forcing conditions (Braconnot et al., 2007; Jansen et al., 2007). Still, problems do exist as exemplified by Ramstein et al. (2007) who shows that the simulated wintertime LGM climate is not as cold as proxy data indicates in a range of AOGCMs in the North Atlantic and European region.

AOGCMs have relatively coarse horizontal resolution limiting their ability to simulate regional scale features of the climate. This is a hindrance when comparing to observations, or proxy data, which are local to their nature. A common way to improve the representation of regional scale climate features in AOGCMs is to use high-resolution regional climate models (RCMs) to improve the representation of regional scale climate features (e.g. Rummukainen, 2010). RCMs give a better representation of local conditions and may increase the utility of local scale observations or proxy data. Jost et al. (2005) found that the wintertime warm bias in Europe was reduced in the downscaling of an atmospheric GCM simulation of LGM climate to 50 km resolution with an RCM, although simultaneously deteriorating the agreement with reconstructed LGM precipitation. However, one cannot expect that high-resolution itself can remove all biases as shown by Jost et al. (2005), who find that the warm wintertime bias over western Europe discussed above remains in two PMIP2 AGCMs and one RCM all run at relatively high resolution (Table 1). Common to previous high-resolution simulations of the LGM climate (Table 1) are prescribed SSTs with no interannual or decadal variability and relatively short time periods (ca. 10 yr). Given the large inter-decadal variability within the LGM climate found by Brandefelt and Otto-Bliesner (2009) in an AOGCM simulation of LGM climate, there is a risk that such short periods are not representative of long-term conditions

The main objective of this study is to perform and evaluate a long-term (i.e. 50 yr) simulation for LGM climate conditions in Europe taking into account both variability in North Atlantic SSTs and sea ice, and regional vegetation in balance with the simulated climate. To achieve this, we use boundary conditions from an equilibrium simulation with a fully coupled AOGCM under forcing conditions representative of the LGM (following PMIP2). An RCM is used to downscale 50 yr of the AOGCM simulation for Europe, enabling studies of the regional climate including its interannual variability. In addition to the climate models, a regional dynamical vegetation model (DVM) is used to provide vegetation consistent with the simulated European LGM climate. The simulated SSTs from the AOGCM are compared to proxy data from the North Atlantic and the Mediterranean. RCM results are compared to terrestrial proxy data for near-surface temperature and precipitation. The simulated vegetation is compared to data on LGM vegetation. Sensitivity experiments are undertaken to investigate the impact of changes in ice sheet configuration and vegetation on the regional climate. In particular, we investigate if these sensitivity experiments lead to differences larger than the uncertainty ranges associated with proxy data. Finally, we make a qualitative estimate of if and how snow will accumulate in the absence of an ice sheet in the RCM simulation. Results of this study may be used as an indication of where an ice sheet could potentially form from local accumulation of snow at LGM.

2. Models, forcing conditions and proxy data

In this section, we first give an overview of the model approach before describing the models and forcing conditions used in the simulations in more detail. We also present the palaeodata used for comparison with the model results. Figure 1 shows the model chain. Fifty years from the AOGCM (CCSM3) simulation was downscaled with an RCM (RCA3) that was first run with present-day vegetation including land-use as a first guess. The resulting climate was then used in the dynamic vegetation model (DVM) LPJ-GUESS to produce new vegetation consistent with the LGM climate. Finally, a repeated RCA3 run with the new vegetation was completed to produce the climate that is used in subsequent analyses. In the same way, two runs with RCA3 were also performed to downscale the 50-yr-long reference simulation with CCSM3 for the recent past climate (representative of year 1990): one using present-day vegetation including land-use, and one using potential present-day vegetation determined with LPJ-GUESS forced by the climate obtained in the first run (Fig. 1).

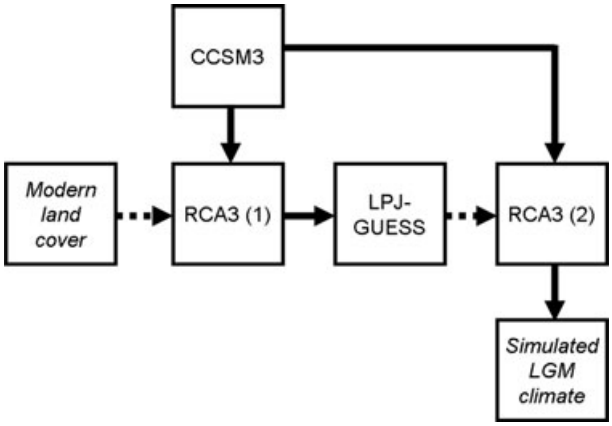

Fig. 1. Setup for the different models: full lines represent the climate simulated by the global (CCSM3) and regional (RCA3) climate models, and dashed lines represent the vegetation needed as input to the regional climate model.

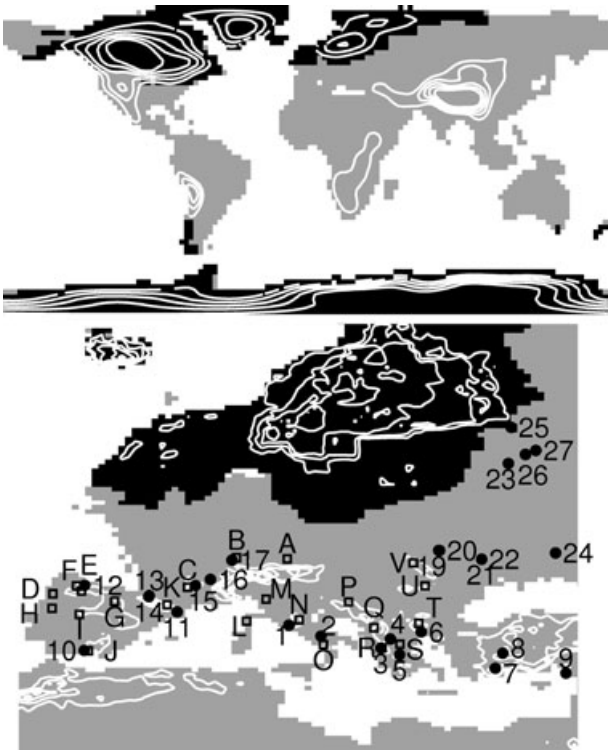

Fig. 2. Land-sea mask (grey), ice sheet extent (black) and orography (white isolines for 1000, 1500, 2000, 2500 and 3000 m) for RCA3 (top) and CCSM3 (bottom). The land-sea mask is taken from the atmospheric part of the models. Indicated as land areas are all grid boxes with a land fraction of at least 20%. Also shown are the locations of the sites for which proxy data have been compared with model results, Wu et al. (2007) are represented by circles and numbers, Allen et al. (2008) represented by squares and letters.

2.1. The CCSM3 global climate model

We use data from the Community Climate System Model version 3 (CCSM3) (Collins et al., 2006). CCSM3, which is an AOGCM, has been tested for the recent past climate, the pre-industrial climate (around AD 1800) (Otto-Bliesner et al*.,* 2006a), the LGM and the Mid-Holocene warm period (6 kyr BP) (Otto-Bliesner et al., 2006b). The atmospheric and land components of CCSM3 in the present simulations were run with the horizontal resolution T42, roughly equivalent to $2.8^\circ \times 2.8^\circ$ latitude–longitude. The ocean and sea-ice components share a horizontal grid of 320×384 points.

Model years 1125–1174 from a nearly 2000-yr equilibrium simulation with CCSM3 for LGM conditions (Brandefelt and Otto-Bliesner, 2009) were used for prescribing boundary conditions in the RCM LGM simulations. The simulation of the recent past climate used here as a reference is a 50-yr-long continuation of a simulation using constant forcing representative of year 1990 described in Collins et al. (2006). Our reference simulation shows a reasonable overall agreement to observations, although regional biases are apparent. For northern Europe, the simulated climate shows local biases of $+1$–4 °C in seasonal mean temperatures and up to $+50\%$ in precipitation compared to gridded climatologies (Kjellström et al., 2009). The relatively large biases in precipitation partly results from the coarse resolution and thereby poor representation of the Scandinavian mountains, which strongly influence the amount of precipitation in that region. All simulations with state-of-the-art global climate models at coarse horizontal resolution show similar biases (Randall et al., 2007).

2.2. The RCA3 RCM

The Rossby Centre regional atmospheric climate model RCA3 (e.g. Kjellström et al*.,* 2005, Samuelsson et al., 2011) was applied for downscaling CCSM3 results to a higher resolution for Europe. RCA3 and its predecessors RCA1 and RCA2 have been extensively evaluated and used for downscaling experiments for the recent past climate and future climate change scenarios (Rummukainen et al., 1998, 2001; Räisänen et al., 2003, 2004; Jones et al., 2004; Kjellström et al., 2011). The ability of the regional model is strongly dependent on the realism of the driving global model simulation (Kjellström et al., 2011). Also, RCA3 has been used in palaeoclimatological applications for downscaling global model data for parts of the last millennium (Moberg et al., 2006) and parts of the Marine Isotope Stage 3 (Kjellström et al., 2010), but never for LGM. Here, RCA3 was run over Europe with a horizontal grid spacing of 0.44° (approximately 50 km) and a time step of 30 min. Figure 2 shows the inner model domain excluding the eight-point boundary relaxation zone. When used to downscale CCSM3, data for initialising RCA3 were taken from CCSM3. After that, at every 6 h of the simulation, RCA3 reads surface pressure, humidity, temperature and wind from CCSM3 along the lateral boundaries of the model domain and also SST and sea-ice extent within the

model domain. All RCA3 simulations have been run with 1-yr spin-up time, after which the atmosphere/land surface system is assumed to have forgotten its initial state.

2.3. The LPJ-GUESS DVM

We used the DVM LPJ-GUESS (Smith et al., 2001) to generate fields of potential vegetation (i.e. the vegetation that would exist in the absence of human intervention) for ice-free land areas in the RCA3 domain. LPJ-GUESS is a process-oriented model optimized for application across a regional grid. The model shares a common plant physiological and biogeochemical core with the global model LPJ-DGVM (Smith et al., 2001; Sitch et al., 2003), widely used in studies of the global carbon cycle and biosphere–atmosphere coupling (e.g. Cramer et al., 2001; Sitch et al., 2005, 2008), but is more detailed and mechanistic in its representation of vegetation structure and dynamics, distinguishing plant populations, age classes, vertical stand structure and patch-scale heterogeneity. This level of detail is arguably necessary to correctly characterize the transient vegetation dynamics under periods of rapid climatic change, such as the present day, which are controlled by population processes operating on similar time scales to the climate change itself. LPJ-GUESS has been evaluated by comparison with observed vegetation patterns and dynamics (Smith et al., 2001, 2008; Hickler et al., 2004; Zaehle et al., 2006; Miller et al., 2008) as well as ecosystem carbon exchange (Morales et al., 2005; Yurova and Lankreijer, 2007; Smith et al., 2008; Wramneby et al., 2008) and has been used to model climate change impacts on European vegetation and ecosystems in a variety of studies (Gritti et al., 2006; Koca et al., 2006; Morales et al., 2007; Wolf et al., 2008).

The input data to LPJ-GUESS from RCA3 include: interannually varying monthly mean precipitation, surface air temperature and incoming shortwave radiation. A spinup of 300 simulation years was performed by repeatedly using the first 30 yr of RCA3 climate data. After that the full 50-yr period was run to generate the LGM vegetation. LPJ-GUESS provides fractional vegetation cover in the classes broadleaf and coniferous forests, open land and bare ground, where open land is defined as areas with some cover of low-stature vegetation such as grasses, herbs, dwarf shrubs or mosses, but devoid of trees. In RCA3, broadleaf and coniferous forests are aggregated for calculation of the forest fraction. However, information about the two classes is kept separate when calculating seasonally varying leaf area index. Open land and bare ground are aggregated into a single open land fraction.

2.4. Forcing conditions

The aim of this study is to simulate the climate under constant LGM boundary conditions and forcing. We take forcing conditions including land–sea distribution, topography, ice sheet extent, atmospheric green house gas (GHG) and aerosol concentrations as constants in time. Also vegetation is treated as a constant in the simulation albeit with a seasonal cycle.

In the CCSM3 LGM simulation, we used insolation of 1365 W m^{-2} and orbital conditions representative for the 21 kyr BP (as described in PMIP2). The same insolation is used in RCA3. Orbital parameters cannot be set in RCA3, why we use conditions reflecting the end of the 20th century. RCA3 has a low sensitivity to the insolation due to the fact that the climate in a relatively small region, such as the RCA3 domain, is to a strong degree governed by the large-scale forcing from the global model.

As stated in the PMIP2 protocol, the GHG concentrations in the CCSM3 LGM simulation were: CO_2: 185 ppm_v, CH_4: 350 ppb_v, N_2O: 200 ppb_v and pre-industrial amounts of ozone, sulphate, dust and sea salt were used. RCA3 uses CO_2-equivalents (CO_2-eq) to account for the total radiative forcing from GHGs and aerosols instead of describing them separately. A CO_2-eq of 168 ppm_v calculated based on IPCC (2001) was used in RCA3 for LGM.

In both CCSM3 and RCA3, ice sheet setup and orography for LGM conditions were taken from the ICE-5G data set (Peltier, 2004) and imposed directly in the models. Kageyama et al. (2006) find that the use of the ICE-5G reconstruction improves the simulated climate in western Siberia in AOGCM simulations as compared to simulations with the earlier ICE-4G reconstruction. Although ICE-5G ice sheets and orography are used in both CCSM3 and RCA3 there are notable differences in orography due to the difference in horizontal resolution. The Scandinavian ice sheet is at least 1000 m higher in RCA3 than in CCSM3 and in southern Europe CCSM3 does not show any mountains higher than 1000 m (Fig. 2). In both models, the ice sheets were treated as ice-covered mountains allowing for variations in snow accumulation.

Present-day bathymetry in CCSM3 was used with the coastline changed according to a 120-m sea-level lowering (Lambeck, 2004). In RCA3 coastlines from ICE-5G were used, implying that some current oceanic areas were instead land areas (Fig. 2).

Vegetation in the LGM simulation with CCSM3 is prescribed according to modern conditions in line with the simulation protocol in PMIP2. Similarly, the vegetation in the first LGM simulation with RCA3 is prescribed according to RCA3 modern conditions, with higher resolution than in CCSM3. In the second run, we use the LPJ-GUESS vegetation as described earlier.

2.5. Proxy data

To evaluate the CCSM3 simulation, we use LGM SST-anomalies w.r.t. the recent past climate. The palaeo data set is the gridded multiproxy approach for the reconstruction of the glacial ocean surface (MARGO, MARGO project members, 2009) that combines 696 microfossil and geochemical reconstructions of summer, winter and annual mean SSTs. The MARGO data representing LGM (defined as the time period 23–19 kyr BP), are

projected onto a regular grid of 5° × 5° resolution. The error estimates for the MARGO SST data are in the range 0.8–9.9 °C, with a median value of 1.95 °C. The error estimates represent 1 standard deviation and thus the probability is 66% (95%) that the SST is within ±1 (2) standard deviations.

Terrestrial proxy data for near-surface temperatures and precipitation are taken from reconstructions based on inverse vegetation modelling starting from data on pollen biome scores (Wu et al., 2007, hereafter referred to as WU07). They give a central value and a 95% confidence limit: for precipitation data they estimate it to be ±60 mm month^{-1}, and for temperature ±10–20 °C in the coldest month and ±3–5 °C in the warmest month. The coldest (warmest) month is defined by WU07 as January (July), which corresponds to what is simulated by the model. We use all data from WU07 within the RCA3 model domain apart from one site in northern Norway that is representative for conditions at 18 kyr BP well after the LGM in that region (Table 2).

An independent set of proxy data for near-surface temperature was presented by Allen et al. (2008, hereafter referred to as AL08). They derive precipitation/temperature relations for mountain regions from degree-day modelling of palaeo glaciers in southern Europe and Russia. They estimate LGM temperatures based on the temperature that is needed to sustain glacier surface mass balance assuming precipitation being reduced with 0%, 40% and 80% compared to modern day precipitation. The resulting data set consists of one temperature estimate per precipitation reduction at each glacier. The precipitation anomaly in our simulations varies horizontally, prohibiting direct comparison with their reconstructions based on horizontally homogeneous precipitation anomalies. To allow comparison, the AL08 temperatures, based on 0%, 40% and 80% precipitation reductions, are linearly interpolated (and extrapolated in the case of RCA3 precipitation outside the range of AL08 precipitation reductions) to represent the same precipitation anomaly as simulated by RCA3 at the specific location. Further, the reconstructed temperatures represent local glaciers in areas of high altitude. The orography in RCA3 is not that detailed and temperature can vary considerably due to height differences. By comparing the equilibrium line altitude (ELA) of the glaciers in the reconstruction by the altitude in RCA3 for the same locations, the temperature is adjusted w.r.t. height using the free atmospheric

Table 2. Data from Wu et al. (2007) (WU07) used in this study

Site	Lon	Lat	Alt	RCA Alt	TCO	TWA	TANN	Pjan	Pjul	PANN
1 Castigl	12.75	41.89	44	419	−9.7	−4.8	−6.6	−24.2	−30.6	−224.8
2 Monticc	15.6	40.94	530	401	−11.3	−2.3	−5.6	−13.6	−27.8	−184
3 Ioannin	20.73	39.76	469	388	−20	−1.2	−8.1	−10.7	−28.3	−273.6
4 Khimadi	21.58	40.61	560	370	−9.8	−2.6	−5.2	−24.3	−16.5	−172.1
5 Xinias	22.26	39.05	500	358	−8.9	−3	−5.2	−19	−22.1	−157.4
6 TenaghP	24.3	41.17	50	365	−6.3	−4.5	−5.1	−2.1	−36.9	−123.4
7 SutG	29.88	37.05	1400	388	−5.5	1.1	−1.2	−20.9	−1.6	−85.5
8 Karamik	30.8	38.42	1000	399	−7.1	−1.9	−3.8	−22.4	12.9	−28.2
9 Ghab	35.3	35.68	300	358	−18.6	−6.8	−11.1	−9.2	−1.2	−22.2
10 Padul	−3.67	37	785	352	−10.8	−4.5	−6.8	−16.8	5.9	−33.2
11 Banyols	2.75	42.13	173	296	−12.2	−4.2	−7.1	−14.7	−5.3	−49.5
12 Ajo	−6.15	43.05	1570	336	−11	−4.2	−6.7	−28.6	−18.6	−163.8
13 Biscaye	−0.17	43.27	410	362	−15.1	−4.3	−8.3	−14.6	−25.9	−278.9
14 Lourdes	−0.17	43.17	430	402	−7.1	−1.7	−3.6	−32.5	−56	−382.2
15 Bouchet	3.67	44.89	1200	428	−8.3	−0.6	−3.3	−31.3	−47	−326.2
16 Echets	4.89	45.67	267	432	−11.4	−7.6	−8.9	−19.4	5.3	−44.5
17 GrandeP	6.5	47.73	330	422	−17.6	−11.8	−13.9	−17	−23.7	−189
19 R054	27.08	48.92	100	402	−11.5	−12.6	−12	−23.5	−13.6	−90.9
20 R056	27.17	48.92	100	393	−11.2	0.4	−3.9	−34.4	−19.2	−129.7
21 R057	31.1	47.65	100	538	−12.8	0.4	−4.5	−16.1	2.7	−14.2
22 R058	31.11	47.65	100	593	−12.3	−0.8	−5.1	−28.2	−6.6	−59.2
23 R003	37.19	56.37	128	393	−12.4	−9.7	−10.5	−23.1	−12.3	−78.5
24 R001	38.35	47.16	38	391	−16.5	−8.7	−11.5	−31.9	−13.1	−76.7
25 R045	39.33	59.7	125	643	−15.6	−7.5	−10.4	−29.9	−23.1	−153.5
26 R002	39.58	56.92	136.8	536	−12.5	−8.8	−10	−23.9	−16.2	−106
27 R046	41	57.08	150	774	−12	−4.1	−7	−21.7	−10.8	−80.4

RCA Alt is the altitude in RCA3 at the grid point closest to the site. TCO, TWA and TANN are temperature anomalies (°C) for, respectively, the coldest and warmest months and annual mean conditions. Similarly, Pjan, Pjul and PANN are the corresponding precipitation anomalies (mm month^{-1}).

Table 3. Data from Allen et al. (2008) (AL08) used in this study

Site	Lon	Lat	ELA	RCA Alt	ATA0	ATA-40	ATA-80	RCA P (%)	RCA ATA	ATA (adj.)
A S. Germany	11.88	48.31	900	700	−12.0	−13.2	−15.3	−39.04	−8.24	−11.87
B Vosges Mnts.	6.87	48.03	700	578	−13.9	−15.1	−17.2	−22.75	−8.90	−13.79
C Massif Central	3	44.63	1100	653	−13.2	−14.5	−16.8	−9.91	−9.12	−10.62
D Sierra de Geres	−8.44	41.57	1000	116	−11.9	−13.5	−16.0	21.19	−8.34	−5.30
E Sierra de Anca	−6.19	42.47	1300	1163	−13.4	−15.1	−17.9	−9.88	−8.23	−12.93
F Cantabrian Mnts.	−6.83	42.82	1500	586	−10.7	−12.2	−14.2	−15.05	−8.67	−5.33
G Si. de la Demanda	−2.97	42.13	1700	1228	−13.5	−14.9	−17.0	3.77	−8.75	−10.30
H Si. De la Estrala	−7.88	40.22	1500	749	−11.6	−13.2	−15.7	67.49	−8.49	−4.02
I Si. de Gredos	−5.4	40.25	1800	575	−14.2	−15.7	−16.6	37.33	−7.43	−4.84
J Sierra Nevada	−3.32	37.05	2200	1408	−15.7	−17.6	−19.7	105.44	−7.12	−5.54
K Pyrenees	1.67	42.68	1500	1608	−11.2	−12.7	−14.6	−39.11	−8.37	−13.37
L Corsica	9	42.0	1600	68	−11.0	−12.2	−13.9	17.51	−8.47	−0.52
M N. Ital. Apenn.	10.4	44.28	1100	60	−13.9	−15.1	−17.3	29.54	−8.43	−6.25
N C. Ital. Apenn.	13.6	42.45	1500	1243	−12.0	−13.1	−15.1	26.48	−8.65	−9.60
O S.Ital. Apenn.	15.85	40.11	1600	293	−12.0	−13.1	−14.7	12.84	−7.35	−3.15
P Croatia, Bosnia	18	44.27	1500	859	−11.6	−13.1	−15.7	−5.27	−6.67	−7.63
Q Albanian Alps	20.23	41.75	1500	200	−12.6	−14.3	−17.2	3.96	−6.48	−3.98
R Epirus Mnts.	20.81	39.78	1700	598	−12.5	−13.9	−15.5	9.58	−6.58	−5.00
S E. Greek Mnts.	22.35	40.08	2100	818	−10.6	−11.8	−13.4	−18.54	−5.42	−2.82
T Rhodopi Mnts.	24.19	42.02	2100	1540	−8.2	−9.4	−11.2	−21.34	−5.54	−5.20
U C. Carpatians	25.2	45.62	1800	1191	−8.0	−9.1	−10.9	−14.73	−6.02	−4.45
V N. Carpatians	24.38	47.87	1500	702	−9.8	−10.9	−12.7	6.16	−7.06	−4.44

The columns represent (1) site, (2) longitude, (3) latitude, (4) average equilibrium line altitude (ELA), (5) altitude in RCA3, (6) annual temperature anomaly (ATA) (°C) with 0% precipitation reduction (PR), (7) ATA with 40% PR, (8) ATA with 80% PR, (9) precipitation anomaly in RCA3 (%), (10) ATA in RCA3 and (11) adjusted ATA from AL08 w.r.t. height and precipitation.

lapse rate as simulated by RCA3. This new temperature adjusted w.r.t. both precipitation and elevation is then compared with simulated temperature (Table 3). We use all AL08 data from within the RCA3 model domain.

3. Simulated climate

3.1. Global LGM climate simulated with CCSM3

The annual global mean surface temperature is 7.9 °C in the CCSM3 LGM simulation, which is 6.9 °C colder than in the CCSM3 simulation of the recent past climate. This response is stronger than in most of the PMIP1 (1.9–9.2 °C colder than in the pre-industrial/recent past climate) and PMIP2 (3.4–5.5 °C colder than the pre-industrial climate) simulations as presented by Kageyama et al. (2006) and Braconnot et al. (2007). Temperature differences compared to the recent past climate are larger at mid and high latitudes in both hemispheres and, due to the increased albedo and surface elevation, most pronounced over the Laurentide and Fennoscandian ice sheets (Fig. 3). Our simulation primarily deviates from the PMIP2 mean (Braconnot et al., 2007, their Fig. 3) over the North Atlantic and North Pacific, differences are smaller over the Laurentide and Fennoscandian ice sheets. The upper-tropospheric circulation difference from the recent past climate is dominated by an amplification of the topographic wave over the Rocky Mountains and the Laurentide ice sheet in winter and with a smaller amplitude also in summer (Fig. 3). These changes are also found in the earlier period of the CCSM3 LGM simulation analysed by Otto-Bliesner et al. (2006). They are associated with a southward shift of the Atlantic and Pacific storm tracks resulting in a decrease in the high-latitude precipitation while mid-latitude precipitation increases in both winter and summer (Fig. 3). This shift in precipitation in the North Atlantic and North Pacific is a common feature in four PMIP2 simulations analysed by Lainé et al. (2009).

Changes in the oceans include a 50% decrease in the strength of the Atlantic Meridional Overturning Circulation and a decrease in annual mean SST with a maximum of 12 °C in the Nordic Seas and northern North Atlantic (not shown). The response of the Atlantic Meridional Overturning Circulation (AMOC) to LGM conditions differs among different PMIP coupled models. The response found in our simulation is relatively strong as compared to the 17% decrease in AMOC strength found by Otto-Bliesner et al. (2007) for the earlier period of this CCSM3 simulation (Brandefelt and Otto-Bliesner, 2009). It is also stronger than what is found in other coupled PMIP simulations. The AMOC slows down considerably (by 20–40%) during the LGM as compared to the modern climate in four PMIP

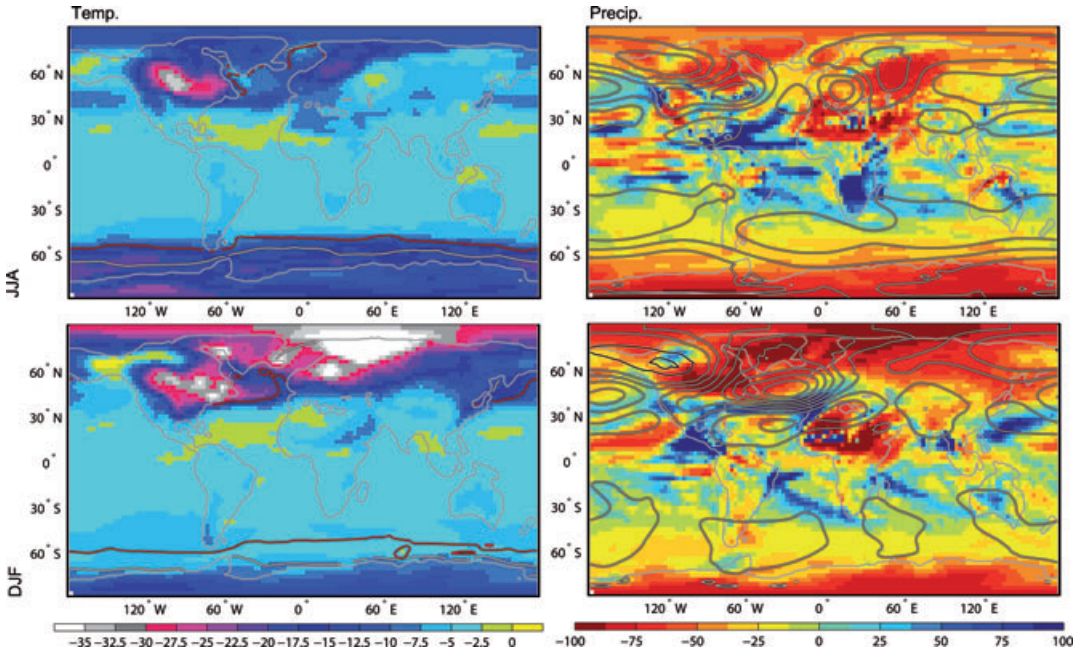

Fig. 3. Summer (June–August, upper panels) and winter (December–February, lower panels) difference between the CCSM3 LGM simulation and the recent past climate. T_{2m} (shading) and fraction of the surface covered by sea ice (contour at 50% sea ice coverage for CCSM3 LGM in red and the recent past in white) is shown in the left panels. Geopotential height at 300 hPa (contours every 50 geopotential meters, gpm) and relative changes in precipitation (shading). Negative geopotential height contours are coloured white and positive are coloured black, the zero contour is omitted. Units are °C and % in the left panels and gpm and % in the right panels.

models, there is a slight reduction in one model and four models show a substantial increase in AMOC strength (by 10–40%) (Otto-Bliesner et al., 2007; Weber et al., 2007).

The large-scale spatial pattern of winter and summer SST differences between the recent past and the LGM has the strongest response around 45°N, along the eastern North Atlantic coast and partly also in the Mediterranean. In the Norwegian Sea, the anomaly amounts to 10–12 °C (Fig. 4). The sea ice cover extends further equatorward in the North Atlantic, North Pacific and the Southern Ocean. The large-scale spatial pattern of winter and summer SST is similar in the different PMIP2 simulations (MARGO Project Members, 2009; their figures S4 and S5). In the Norwegian Sea, however, the magnitude of the anomaly varies among the PMIP2 simulations with a winter and summer cooling of 0–8 °C.

The spatial pattern of the temperature anomaly in the North Atlantic and Nordic Seas coincides with the pattern of sea ice growth (not shown), i.e. the largest anomalies occur in the regions of more sea ice compared to recent past climate and smaller anomalies occur in regions that experience extensive sea ice already in the recent past climate. The same pattern in SST anomalies can be seen in the proxy data, but they also indicate that the summer and winter SST was possibly as warm or even warmer during LGM than in the recent past in parts of the Nordic Seas (Fig. 4). As shown in Fig. 4, the CCSM3-simulated LGM SST falls within ±2 standard deviations of the MARGO proxy SST for most grid boxes in the North Atlantic region in both summer and winter. For the remaining grid boxes, CCSM3 more often shows anomalies that are colder than indicated by the MARGO proxy data. Therefore, we conclude that CCSM3-simulated LGM SSTs are possibly too low in this region.

CCSM3-simulated LGM SST falls within ±2 standard deviations of the MARGO proxy SST for most grid boxes also in other regions of the globe (not shown). The MARGO data indicates moderate anomalies in the tropical SST (less than ±2 °C), whereas the CCSM3 LGM-simulated SSTs are colder than in the recent past climate by 2–4 °C. An average of PMIP2 tropical SSTs are 1.0–2.4 °C colder than pre-industrial values (Otto-Bliesner et al., 2009). The largest anomaly in the Southern Hemisphere found in the simulated LGM climate occurs around 50°S, which is colder by 2–8 °C in summer and winter. This anomaly occurs, similar to the Northern Hemisphere, in regions where the sea ice extent is increased. There is an indication also in the MARGO proxy SST data of regions of maximum differences compared to present-day conditions in the Southern Hemisphere around 50 °S in summer (January–March), whereas in winter (July–September) there are too few data points in this region to compare.

Sarnthein et al. (2003) conclude that sea ice only covered the Arctic Ocean and the western Fram Strait during LGM summer based on proxy data of SST. In contrast, sea ice spread far south across the Iceland Faroe Ridge during LGM winter. As compared

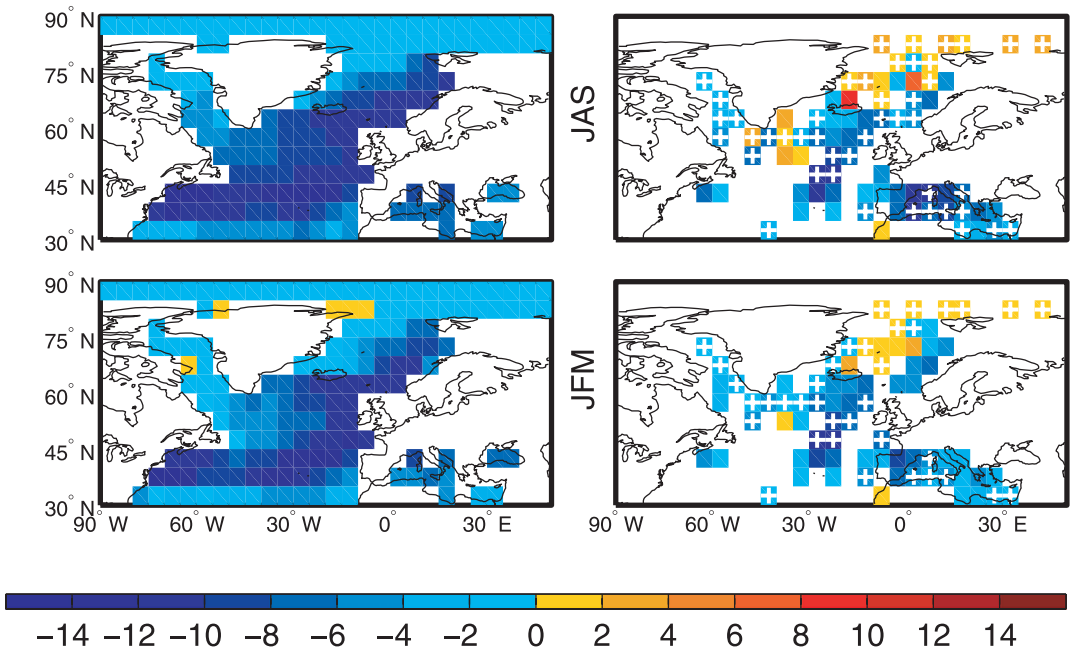

Fig. 4. Summer (JAS, top) and winter (JFM, bottom) mean SST anomalies (LGM minus recent past) for the CCSM3 LGM simulation (left panel) and the MARGO compilation (right panel). The CCSM3 SSTs have been interpolated onto the same grid as the MARGO data. Grid boxes for which the CCSM3 simulated LGM SST falls within ±2 standard deviations of the MARGO proxy SST are indicated with white + signs in the right panels.

to the proxy sea ice estimates made by Sarnthein et al. (2003), the CCSM3 LGM gives too much sea ice in the Labrador Sea and off the New Foundland coast in summer and too much ice in the central North Atlantic in winter (not shown).

Regardless of possible biases in SSTs, the simulated anomalies in annual mean temperatures over Europe in CCSM3 are similar to those obtained in the high-resolution atmosphere—only CCM3—simulations by Kim et al. (2008). They used proxy-based reconstructions of the SST as a lower boundary condition to their simulation indicating that the possible SST bias we report on here does not have a major influence on the annual mean temperature conditions over Europe. Similarly, Kageyama et al. (2006) reported that the relationship between SST anomalies in the North Atlantic and surface temperature anomalies over Europe is not straightforward for the warmest month of the year. They only found a significant relationship between anomalies in the western European region and the North Atlantic for temperatures of the coldest month.

3.2. *European LGM climate simulated by RCA3*

The very cold simulated LGM climate, with annual mean temperatures below 0 °C in all of Europe north of about 50°N and also in high-altitude regions in southern Europe, is clearly seen in Fig. 5. In winter, the situation is even more striking with the 0 °C line encompassing basically all of continental Europe and monthly mean temperatures below −40 °C over the northern parts of the ice sheet. These very large differences are partly due to the perennial snow/ice cover but also to a consequence of the high elevation of the ice sheet. During summer, the area with the lowest temperatures is more confined to the ice sheet, the extent of which is readily visible in Fig. 5. In ice-free parts of Europe temperature anomalies are stronger in the west as a consequence of the low SSTs in the North Atlantic in combination with the influence of prevailing northwesterlies in this region (Fig. 6). In winter when most parts of Europe are snow covered, the north–south gradient is less pronounced.

Compared to the three high-resolution LGM simulations by Jost et al. (2005), the RCA3 results compares best with the HadRM simulation with a deviation of at most 3 °C (the other two being at least 5 °C warmer) in terms of temperature of the coldest month, at least for southern and central Europe. In northern Europe, the signature of temperature anomalies of the coldest month are different. While in RCA3 the maximum negative anomaly is over the ice sheet, all simulations in Jost et al. (2005) have maximum negative anomaly over the ocean. For annual precipitation RCA3 compares best with the LMDZHR simulation, which gives a similar pattern of precipitation anomaly. CCSR1 does not give enough details and HadRM simulates much more precipitation around the coastlines in southern Europe.

The RCA3 results from regions outside the ice sheet are compared with pollen-based proxy data of temperature differences with respect to the present climate from WU07 and the adjusted glacier temperatures from AL08 (Figs 5 and 7). For annual mean temperature, the difference between model and proxies is smaller than 2 °C in Spain, Italy and Greece. In the Alpine

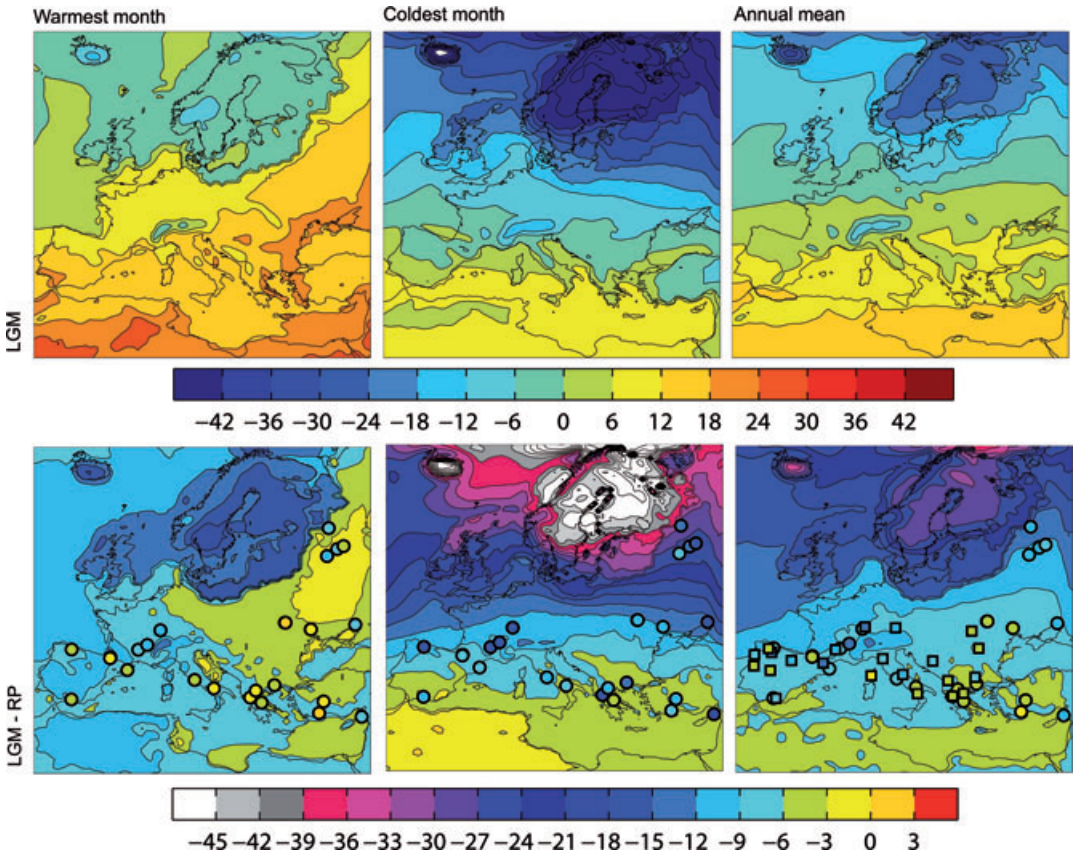

Fig. 5. Mean temperatures of the warmest month, coldest month and year (top). In the lower row differences compared with recent past conditions are shown. Also shown are estimates of temperature anomalies based on proxy data (coloured circles (Wu et al., 2007) and squares (Allen et al., 2008). Unit: °C.

region, good agreement is seen for one of the records whereas RCA3 is warmer than indicated by the other proxies. In the Pyrenees, RCA3 is colder than the proxies. In Turkey, one proxy data is much warmer and one much colder. Compared to AL08, RCA3 simulates annual temperatures within the error bars for most locations, but tends to underestimate temperatures at the northernmost locations. We note that most proxy points are in close vicinity to high-altitude complex terrain areas such as the Alps and the Pyrenees making comparisons with the model results difficult.

For the coldest month, large differences of more than 10 °C between model and proxies are seen in the four records in north eastern Europe (Fig. 7, middle). RCA3 tends to simulate a smaller anomaly in temperature than proxies indicate, but shows a fair agreement (mostly within a few degrees) in the southern half of Europe. There are some notable local exceptions to this where the model shows anomalies 15 °C smaller than the proxies (e.g. in Greece and Cyprus). However, the disagreement is not more than 5 °C for the sites in the surrounding regions implying that these specific sites may not be representative of the larger regional scale. We also note that as the uncertainty ranges in the proxy data are very large, the model-simulated temperatures are within the uncertainty estimates at all but three sites in northeastern Europe.

For the warmest month, the uncertainty ranges in the proxy records are much smaller than in winter. This means that the comparison between model and proxies has the potential of being more useful than in winter for which uncertainties are very large. RCA3 shows a larger anomaly in temperature than the proxies do at a majority of the locations, most notably in the Mediterranean region (Fig. 7, left), this may be a consequence of the low SSTs in the North Atlantic as simulated by CCSM3. At the same time, RCA3 is warmer than indicated by the proxies in eastern Europe.

Another way to evaluate simulated temperatures is to look at the extent of permafrost. Based on model simulations compared with temperature reconstructions, Renssen and Vandenberghe (2003, hereafter RV03) defines the southern limit of continuous permafrost as the line where the maximum annual mean temperature is below −8 °C and the mean winter temperature below −20 °C. Further, discontinuous permafrost develops when mean annual temperatures are −4 °C or below. The 0, −1, −4 and −8 °C isotherms for annual mean temperatures are similar in RCA3 to those in their reconstruction (not shown). The −20 °C

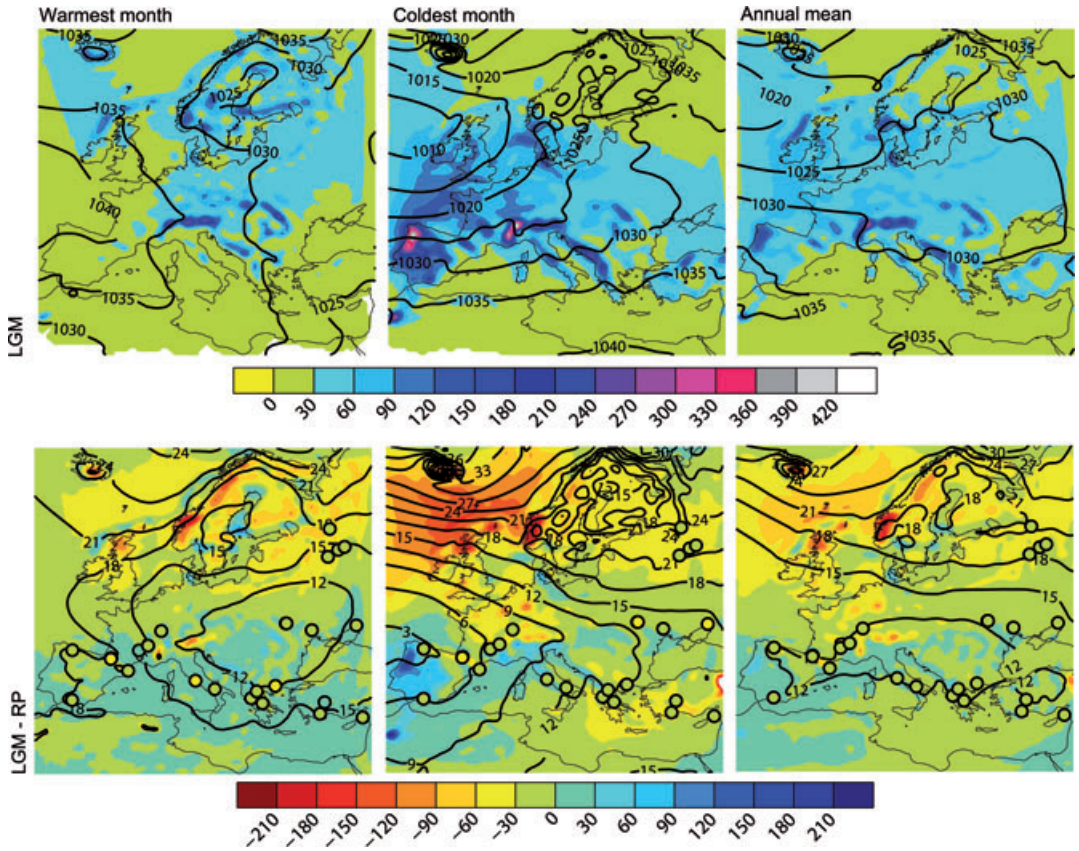

Fig. 6. Mean sea-level pressure (MSLP) and precipitation of the warmest month, coldest month and annual mean (top). In the lower row differences compared with recent past conditions are shown. Shown as coloured circles are precipitation estimates based on proxy data (Wu et al., 2007). Units: hPa for MSLP and mm month^{-1} for precipitation.

isotherm for winter temperatures, on the other hand, is located further to the north in RCA3 in the North Sea/British Isles region implying that continuous permafrost would be less extensive and that RCA3 is possibly too warm in winter in this area. At the same time, however, the SSTs in RCA3 are roughly in agreement with the prescribed SSTs used by RV03 and colder compared to MARGO SSTs (cf. Fig. 4), indicating that any possible warm bias in parts of western Europe is not caused by biases in SSTs in the North Atlantic. Roche et al. (2006) estimates permafrost extent based on simulated temperature and gets about the same extent as RCA3.

Annual mean precipitation in RCA3 shows a broad maximum over the North Atlantic and the European continent (Figs 6 and 7). In winter, the differences w.r.t. the recent past climate resemble those in the annual mean but they are more pronounced. This means mostly dry anomalies, except in the Iberian Peninsula, the southern Alps and Italy (Fig. 6) where more precipitation is simulated in connection to the southward shift in the Atlantic storm tracks discussed earlier. The steep coastlines of western Fennoscandia and Scotland which today are facing the ocean and therefore get a lot of precipitation were, at the LGM, parts of the ice sheet that extends westward. Without the coastline orographic effect, precipitation is much smaller in these regions (Fig. 6). An area with more precipitation than in the recent past climate is the area of what is today the Baltic Sea. During the LGM, this area was an elevated part of the ice sheet in which RCA3 produces relatively large amounts of precipitation during summer.

All proxy data for precipitation are confined to southern Europe. A majority of the sites show reduced precipitation at the LGM for both summer and winter (Fig. 6), although the uncertainties are large, as described earlier. In terms of annual mean precipitation, model and proxy-based data agree fairly well on a decrease of around 300 mm yr^{-1}. For the coldest month of the year, proxy-based data indicate small differences in precipitation compared with the recent past climate. The model, on the other hand, shows a spread with increased precipitation at some sites and decreases at others. Summarizing, for most of the sites, the model is within the uncertainty ranges defined for the proxies. However, there are exceptions to this relatively good agreement, as exemplified by site number 7 in southern Turkey. For this location, there is a large difference in altitude (about 1000 m, Table 2) between the actual site and the model grid elevation, as this is an area of strong gradients in topography. As RCMs, at the

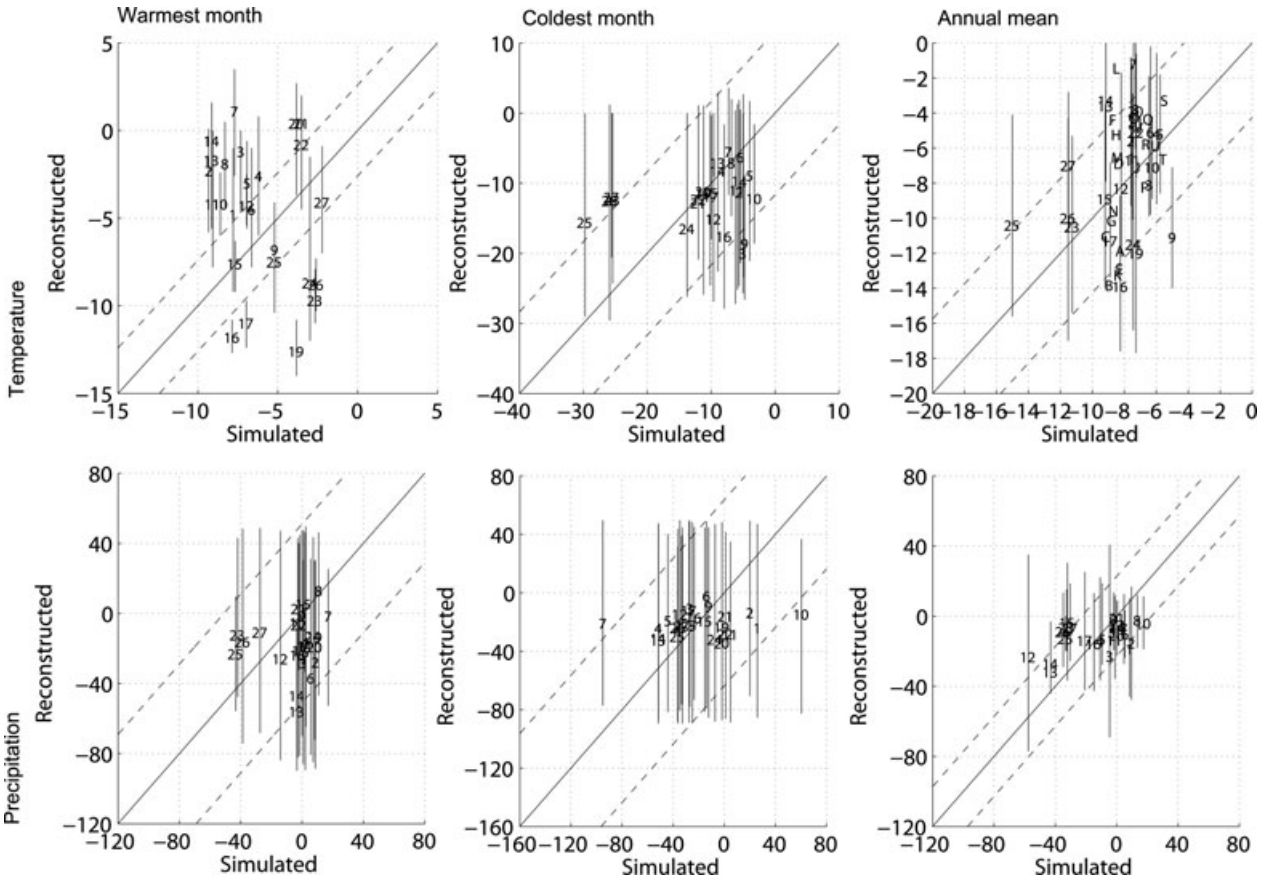

Fig. 7. Comparison of simulated temperature (top) and precipitation (bottom) (horizontal axes) with proxy data (vertical axis) for the warmest month of the year (left), the coldest month of the year (middle) and annual mean (right). The vertical bars illustrated for the proxy data define the 95% confidence levels. The dashed lines represent the average of these errors. The numbers and letters corresponds to the specific sites in Fig. 2. Unit: °C for temperature, mm month^{-1} for precipitation.

horizontal resolution we use here, cannot simulate local details of precipitation in mountainous areas, the large differences may be more of a representativity problem than an actual bias. It can also be noted from Fig. 6 that the pattern in precipitation change is noisy in its nature and that relatively small horizontal offsets from the sites may alter the correspondence between model and proxies.

Kuhlemann et al. (2008) study the change in difference between ELA temperature and SST between LGM and present-day conditions in the Mediterranean region. They suggest that the atmospheric lapse rate in parts of that area was noticeably steeper (8.5–10 °C km^{-1}) at LGM than today leading to more unstable conditions. This reduction in stability, in combination with intrusions of cold air from the north, would favour convective precipitation in the southern Alps, Apennines and Dinarides; especially on the upwind flank of the mountain regions. Our simulation shows 25–50% more precipitation than in the simulated recent past on an annual mean basis in these regions, possibly supporting their suggestion. The lapse rate is steeper in the LGM simulation than in a corresponding simulation of present-day conditions in large areas around the Mediterranean for most of the year; although statistically significant, the difference is small (0–0.4 °C km^{-1}). This indicates that the increased precipitation in these areas are not only a result of stronger convection, at least not in the model. In northern Europe the simulated LGM lapse rate is weaker (1–2 °C km^{-1}) indicating more stable conditions, especially in winter (Fig. 8).

3.3. *European LGM vegetation simulated by LPJ-GUESS*

The vegetation model simulates vegetation reminiscent of tundra and/or montane woodland over ice-free parts of central and southern Europe (Fig. 9). Short, cool summers and low CO_2 concentrations limit primary production and tree growth. Boreal needle-leaved trees dominate the tree canopy in the more continental climate of eastern Europe, whereas low growing season heat sums limit establishment to broadleaved deciduous trees of the mountain birch type in western Europe.

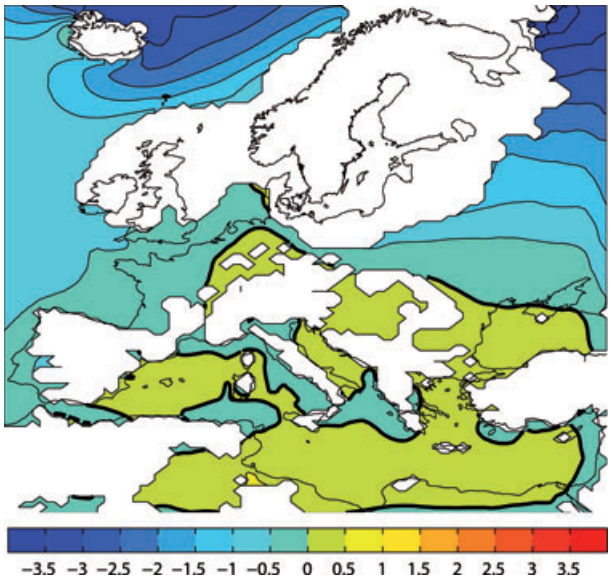

Fig. 8. Difference in annual average atmospheric lapse rate (difference between 700 and 900 hPa levels) between the LGM simulation and the simulation of the recent past, ice sheets and areas with elevation higher than 500 m are masked out. Units: $^{\circ}$C km^{-1}.

A pollen-based reconstruction of vegetation in ice-free parts of Europe at LGM indicate that forested areas were more or less absent (Harrison and Prentice, 2003). This is supported by a reconstruction based on a wider range of different data including both pollen data and plant macrofossils (Ray and Adams, 2001). Both these studies suggest that central and southern Europe instead was dominated by steppe or dry shrubland vegetation. Much lower rainfall than today and reduced plant water-use efficiency associated with lower CO_2 concentrations in the atmosphere have been invoked as causes of low plant-available moisture that would limit the occurrence of trees in favour of grasses (Harrison and Prentice, 2003). The semi-open landscapes simulated by LPJ-GUESS over parts of Southern Europe suggest a greater representation of trees than the data-based reconstructions. A study using an equilibrium biosphere model based on a range of GCM-reconstructed climates likewise suggests the presence of boreal forest vegetation over southern Europe at LGM (Kaplan et al., 2003). Biases are possible in both the models and the data-based reconstructions; however, one likely explanation for this discrepancy is that the cold distributional limits for trees in the models are calibrated to the observed modern distributions of dominant taxa in relation to coldest month mean temperatures. The physiological control of these limits is, however, more closely tied to absolute minimum temperatures, representing extreme cold events that result in meristematic freezing and plant death (Woodward and Williams, 1987). Although absolute minimum and coldest month mean temperatures are correlated with one another, the difference between them is likely to have been larger during LGM compared with today's climate. This is supported by the simulated LGM climate (not shown explicitly, but see, e.g. the increased winter time variability in Fig. 13). This will tend to result in a coldward bias in the simulated distributions of tree taxa at LGM. It should also be noted that LPJ-GUESS was not set up to simulate shrubs in this study; LPJ-GUESS was applied with the minimum number of PFTs necessary to represent biogeographic patterns and shifts of relevance for accounting for land–atmosphere feedbacks in the context of our study. Although shrubs can be represented in LPJ-GUESS, tree PFTs with corresponding phenology and bioclimatic constraints provide a sufficient proxy for the purposes of our study (see also Smith et al. 2011).

Consequently, the simulated woody vegetation may also be considered to represent shrubland and woody tundra which were elements of the European vegetation during the LGM (Harrison and Prentice, 2003).

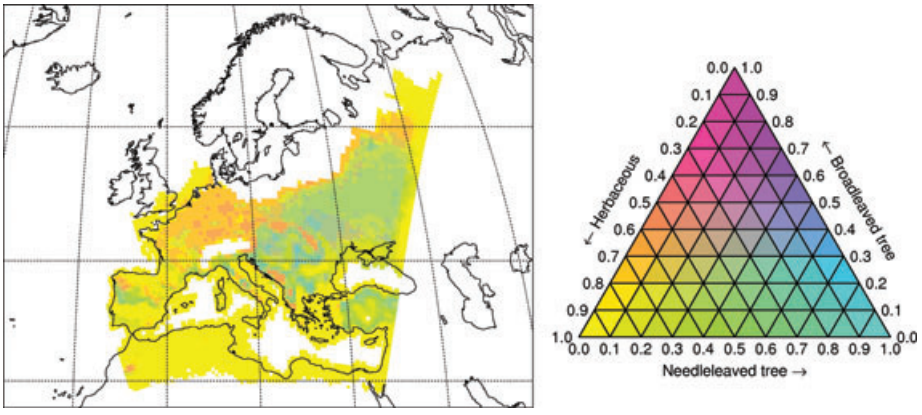

Fig. 9. Proportion of vegetation cover comprising broadleaved trees, needle-leaved trees and herbaceous vegetation resulting from the LPJ-GUESS simulation forced by the initial climate from RCA3. The numbers indicate the fraction of a certain type of vegetation in the vegetated part of each grid box.

4. Discussion

4.1. General uncertainty of the presented results

The major uncertainties in the simulated LGM climate are related to forcing conditions, model formulation and natural variability. The prescribed forcing conditions contain uncertainties related to, among others: vegetation cover, ice-sheet extent and altitude, sea level and aerosol content of the atmosphere. Earlier studies have tested forcing conditions that are more in line with what is expected for the LGM than those used in the PMIP2 protocol, including LGM vegetation (Jahn et al., 2005), LGM mineral dust concentrations (Mahowald et al., 2006), or both (Schneider von Deimling et al., 2006). These three studies indicate that the inclusion of vegetation and dust leads to lower temperatures [for vegetation with 0.6 °C according to Jahn et al. (2005) and with 0.5–1.0 °C according to Schneider von Deimling et al. (2006); for dust with 0.85 °C according to Mahowald et al. (2006) and with 0.5–1.5 °C according to Schneider von Deimling et al. (2006)]. These, and other uncertainties related to forcing conditions and model formulation, could be elaborated more upon in future studies with additional sensitivity experiments.

The issue of natural variability pertains to the simulations with the RCM as we have chosen to downscale periods of limited extension (50 yr). Downscaling of other 50-yr periods from the CCSM3 simulation would not give identical results. The influence of the choice of this specific 50-yr period is determined by computing the time series of the 50-yr running annual mean for the last 1000 yr of the CCSM3 simulation. The time standard deviation of this time series is less than 0.3 °C for T_{2m} for all grid points in Europe and mostly less than 20–40 mm yr^{-1} (locally 50–60 mm yr^{-1}) for precipitation. Based on these relatively small differences between different time periods, we conclude that the 50-yr period chosen from the quasi-equilibrium of the global model is long enough to exclude any major differences due to decadal natural variability and is a good representative of the longer global simulation. Our results also indicate that shorter simulation periods may be problematic as the interannual and interdecadal variability is large. Analogously to the 50-yr running annual means, we calculated 3-yr running annual means for all 3-yr periods within more than 500 yr of the global model. In this case, standard deviations of up to 1.5 °C in near-surface temperature were obtained for parts of western Europe and the North Atlantic between different periods.

An additional source of general uncertainty lies in our approach that is based on the assumption of a climate in quasi-equilibrium, whereas it may be questioned to what degree the real climate approached quasi-equilibrium during LGM. If the real climate system was not in balance and hence not in quasi-equilibrium during LGM we may expect that a balanced state from a simulation is not the best representation of the climate system.

4.2. Sensitivity of the regional climate to vegetation cover

We investigate how a profound difference in regional vegetation would influence the regional LGM climate in Europe by performing an additional experiment with RCA3. This run with RCA3 was done with the same LGM set up as described above apart from the vegetation that is replaced by potential vegetation corresponding to recent past conditions. This potential vegetation was simulated by LPJ-GUESS using RCA3 data from the recent past simulation. It is characterized by deciduous forests in most of central Europe, needle-leaved forests in eastern and northern Europe and herbaceous vegetation in southern Europe (not shown). This is in stark contrast to the simulated LGM vegetation described above (cf. Fig. 9). A comparison of the two RCA3 simulations of LGM climate with different vegetation shows that the simulated regional climate patterns in parts of Europe are sensitive to feedbacks from such large differences in vegetation. The differences in temperature are largest in March, 1–3 °C, close to but outside of the ice sheet and in the Alpine region (Fig. 10). The differences are due to the less extensive forests in the LGM simulation (i.e. reduce forest fraction from around 70% to 30%), leading to higher albedo and thereby lower temperatures. In summer, the differences in temperature are within ±1 °C. We note that despite the radically changed vegetation, differences between the two simulations are small compared to the uncertainties in the proxy data for near-surface

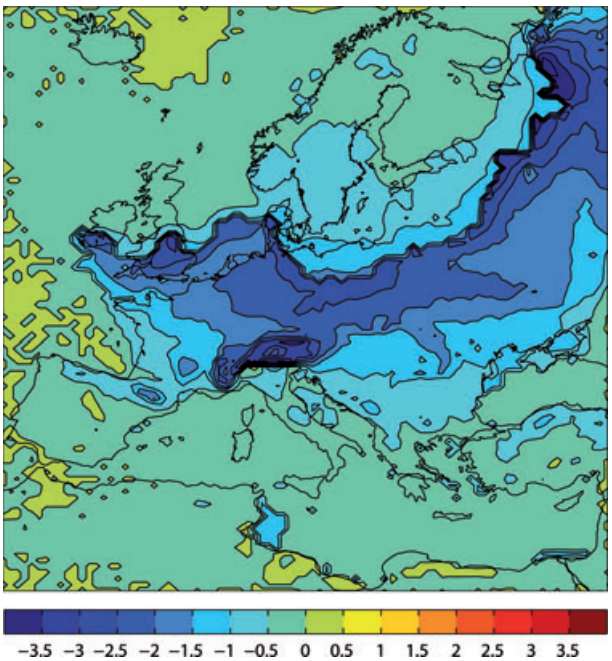

Fig. 10. Temperature difference in March between the reference LGM simulation with LGM vegetation and the LGM simulation with potential vegetation representative of the recent past climate. Unit: °C.

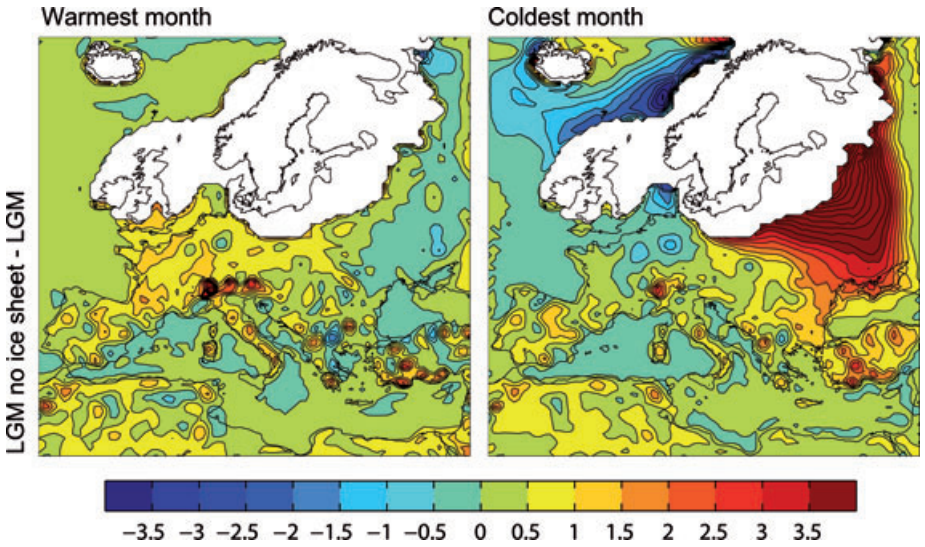

Fig. 11. Comparison of simulated temperature between a simulation of LGM climate without ice sheet and our reference LGM simulation. Unit: °C.

temperature and precipitation. The implication of this is that inferences about LGM vegetation from an RCM-simulated climate cannot be made unless the RCM is evaluated against less uncertain proxy data.

4.3. *Sensitivity of the regional climate to the extent of the ice sheet*

To test the influence of the ice sheet on the local scale, the ice sheet was completely removed in RCA3. For computational reasons, the forcing from CCSM3 was the same as in the previous run. Therefore, the results in this experiment only holds for Europe with the caveat that the large-scale atmospheric features might be different if the ice sheet also would be removed from CCSM3. In this experiment, the winter temperatures are higher by up to 25 °C at the location of the LGM ice sheet (or where the ice sheet used to be), with largest differences in the areas where the difference in altitude with or without an ice sheet is largest; in summer differences are 10–15 °C (not shown). In large parts of western Europe, summer temperatures are higher by around 1 °C, and in winter eastern Europe is 5–10 °C warmer (Fig. 11). A reason for these temperature differences is the warmer conditions in the north and consequently less pronounced outbreaks of cold air masses from these areas. Precipitation in this sensitivity experiment differ from that in the reference LGM simulation by locally up to ±80 mm month^{-1}, where the ice sheet is removed. Outside of this region precipitation differences are mostly within ±10 mm month^{-1}, with only a few scattered, small areas with differences of ±80 mm month^{-1} (not shown).

These results show that the location and extent of the ice sheet has an impact on the simulated RCA3 climate on a local scale: at the ice sheet and in the close vicinity. Effects farther away are mostly seen in eastern Europe in winter, on the 'lee-side' of the atmospheric flow. In summer, impacts of the ice sheet are smaller and we note particularly that there are no differences between the two simulations in eastern Europe. This indicates that the possibly too warm conditions in that area (cf. Fig. 5) are not caused by errors in the location of the eastern margin of the ICE-5G ice sheet unless it is located way too far to the west.

4.4. *Implications for ice sheet extension and growth*

In our LGM simulation snow is accumulating, over the simulated 50-yr period, in three areas: Iceland, Fennoscandia and the Alps (Fig. 12, red line). Because RCA3 does not include dynamic ice sheets, we cannot give details on the extent of ablation zones or

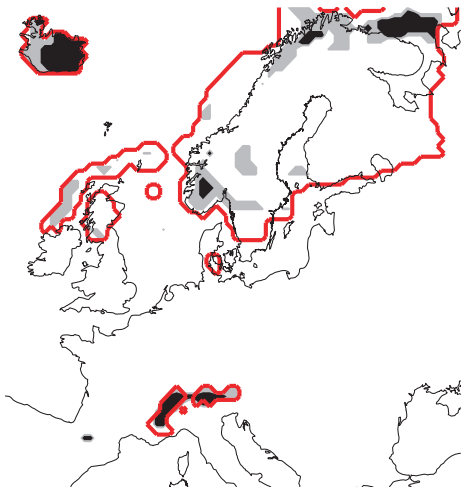

Fig. 12. Areas of snow accumulation in three experiments: (i) the main simulation with LGM topography (red line), (ii) LGM topography but no ice surface (grey shading) and (iii) present-day topography (black shading).

expanding glaciers due to accumulation in the glaciers' central parts. Based on the results we do get, we can nevertheless make some very qualitative statements on the extent of the ice sheet: (i) The climate is warm enough in southern Europe to prevent the ice sheet expanding in this direction. (ii) The climate in northern Europe, over the ice sheet surface, is cold enough to sustain the ice sheet. Monthly mean temperature seldom rises above 0 °C, and over most parts of the ice sheet at least 70% of the precipitation falls as snow. If 60–100% of the precipitation accumulates on the ice sheet it would grow with 0.3–0.5 m yr^{-1} of water equivalents. (iii) Precipitation in the northeastern part of the Fennoscandian ice sheet is very low, indicating that only limited ice sheet growth was possible in that region. This is in general agreement with the findings of only a small extent of the LGM ice sheet in the Ural region in Russia as presented by Mangerud et al. (2008).

In an additional experiment keeping the LGM orography, but replacing the prescribed ice on the surface with bare ground, we investigate if, and in that case where, high altitudes are sufficient to initiate snow accumulation at LGM. Here snow accumulates primarily in the Alps, Iceland and the southern tip of Norway; and to a lesser degree in other elevated parts of Scandinavia and the northwest coast of the British Isles (Fig. 12, grey shading). In a third experiment with present-day topography, snow accumulation occurs at a slower rate and at fewer locations, mostly Iceland and the Alps (Fig. 12, black shading). The results show that both ice on the surface and high elevation is necessary to get snow accumulation in Fennoscandia even with the cold LGM conditions.

4.5. Variability in LGM

Kageyama et al. (2006) discuss how representative proxy data are. They suggest that proxies could be sensitive to extremes as well as to the long-term average climate differences and that different variability at the LGM and today could bias the reconstructions. Ramstein et al. (2007) experiments with temperature and precipitation variability in vegetation modelling. They find that changed variability has a clear impact on the simulated vegetation. The interannual variability at LGM in our simulation is different from that in the recent past climate: the standard deviation of the winter temperature is up to 3 °C higher for central and northern Europe, and over the North Atlantic up to 12 °C higher, mostly due to the presence of sea-ice in this area (Fig. 13). In summer, standard deviation of the temperature is about the same in LGM and the recent past (not shown). The standard deviation of precipitation is higher by 0–20 mm $month^{-1}$ in areas with more precipitation and lower by 10–30 mm $month^{-1}$ (up to 50 mm $month^{-1}$ in mountainous areas) in areas with less precipitation in both summer and winter (Fig. 13). The results indicate that if proxy-based estimates are made assuming present-day variability (or extreme conditions) biases may occur.

4.6. Comparison between the global and regional models

The orography in RCA3 is more detailed than in CCSM3, differences in altitude of more than 1000 m are seen at many locations (cf. Fig. 2). These differences in orography lead to differences in the simulated climate. The higher altitude in RCA3 gives lower temperatures in the mountain ranges compare to CCSM3. Conversely, higher altitudes by some 200–400 m outside the mountainous areas in the smoother CCSM3—orography lead to lower temperature in CCSM3. The smoother orography in CCSM3 also gives temperature and precipitation fields with lower horizontal variability than RCA3. Still, the correlation in monthly values between simulated climate in CCSM3 and RCA3 is high. The correlation varies between regions and seasons but ranges between 0.73 and 0.97 for temperature and 0.54 and 0.96 for precipitation.

Mean absolute errors (MAE) between proxy data (WU07 and AL08) and the global and regional models are presented in Table 4. For RCA3, temperature errors ranges between 2.5 and 5.5 °C depending on season. For the warmest month, this error is about the same size as the proxy data uncertainty range (Table 4). For the coldest month, the error is within the uncertainty range. For precipitation a MAE of 15–23 mm $month^{-1}$ is within the uncertainty range. The differences in MAE between RCA3 and CCSM3 are small for both temperature and precipitation.

5. Summary and conclusions

This work presents results from a 50-yr period in a stabilized LGM simulation with a fully coupled AOGCM (CCSM3). Dynamical downscaling to 50 km horizontal grid spacing for Europe has been performed with the RCA3 RCM. The global model followed PMIP2 forcing conditions, including modern day vegetation and prescribed LGM ice sheets. Regionally, vegetation consistent with the simulated regional LGM climate has been produced for Europe by a DVM (LPJ-GUESS). Subsequently, this LGM vegetation was used in the RCM in a second simulation for which the climate is analysed and compared to existing proxy data. Additional experiments have been undertaken, investigating the sensitivity to type of vegetation and extent of ice sheets.

Given forcing conditions from PMIP2, CCSM3 produces a reasonable climate that is in broad agreement with most of the available SST reconstructions for LGM conditions on a global basis. In the North Atlantic region, this also applies for about half of the proxy records considered. For the remaining records, the model results fall outside of their associated error bars; either as warm or as cold biases. The overall tendency here is that cold biases dominate in the Atlantic close to Europe and in the Mediterranean Sea, both for summer and winter conditions.

RCA3 simulates a cold and dry climate in Europe for LGM. An exception to the dry climate is the Mediterranean region

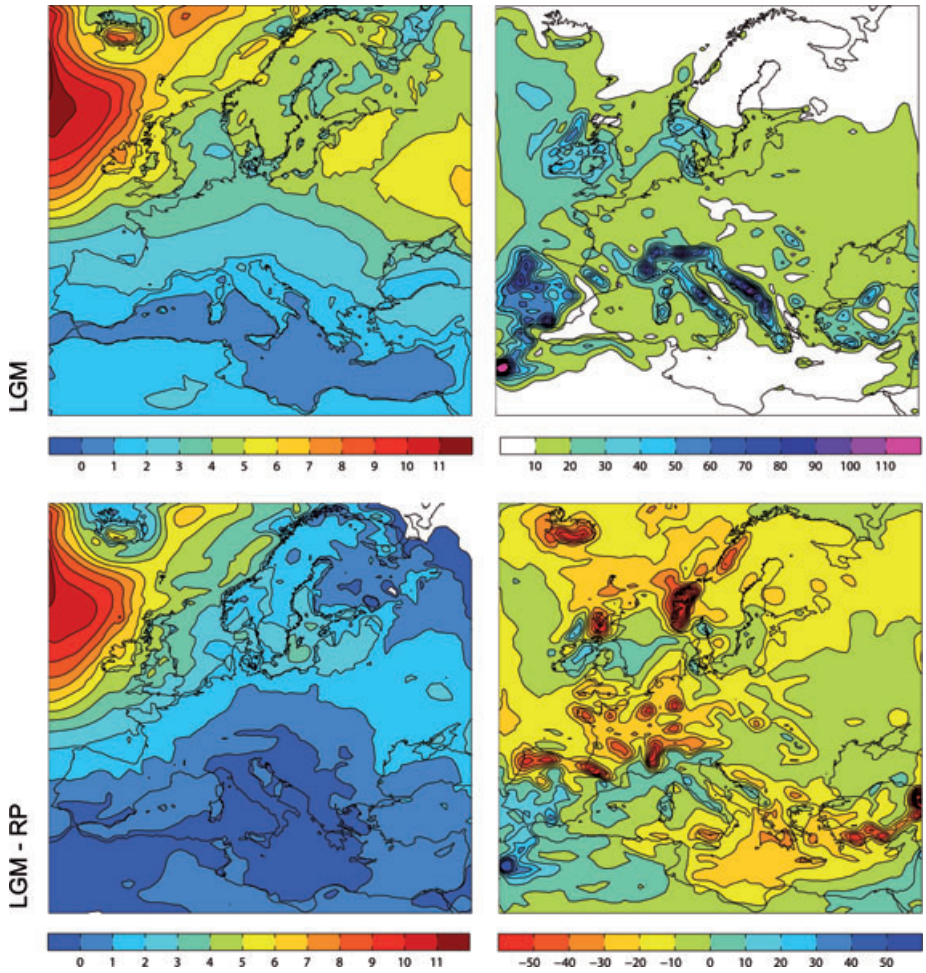

Fig. 13. Top panel: simulated inter-annual standard deviation at LGM; bottom panel: difference in interannual standard deviation between the LGM simulation and the simulation of the recent past, for temperature (left panel) and precipitation (right panel). All panels show winter conditions. Units: °C for temperature, mm month^{-1} for precipitation.

Table 4. MAE between proxies and model for CCSM3 and RCA3 for annual mean (ANN), coldest month (CO) and warmest month (WA)

Variable	Time	MAE		Mean proxy uncertainty	No. of points
		CCSM3	RCA3		
Temperature	ANN	2.9	2.5	8.5	48
	CO	5.8	5.5	23	26
	WA	4.6	4.7	5.2	26
Precipitation	ANN	11	15	46	26
	CO	25	23	127	26
	WA	13	21	101	26

where precipitation is not that different from that in the recent past climate as a result of the simulated southward shift of the storm tracks in CCSM3. The mean absolute difference between proxies and simulated climate is 2.5–5.5 °C for temperature and 15–23 mm month^{-1} for precipitation calculated as averages over all available records. The mean absolute differences between simulated temperature and proxies are about the same for summer and winter. For summer, most simulated temperatures fall outside of the uncertainty range of the proxies. Comparison with the available proxy data in central and southern Europe suggests that the simulated summer climate is too cold there. This may be a result of the cold SST bias over the North Atlantic in CCSM3. In eastern Europe, warm biases dominate in the few available records during summer. For winter time temperatures, most simulated temperatures fall within the uncertainty range of the proxies. The only exception is in the northeast where cold biases are seen at some locations.

The two LGM experiments with different vegetation cover (potential recent past and potential LGM, respectively) show differences of up to 1–3 °C in monthly mean temperature during parts of the yr in some areas. This show that regional vegetation features are important for the regional climate and should

preferably be included in RCM simulations. The results of the iterative simulations with the RCM and DVM show that this is a viable approach, as the resulting vegetation is close to the vegetation in LGM as estimated by other models (e.g. Kaplan et al., 2003). Compared to pollen-based reconstructions, LPJ-GUESS overestimates the woody element of vegetation in eastern and southern Europe.

The resulting climate is in qualitative agreement with the imposed extent of the ice sheet over northern Europe during LGM. Given the prescribed ice sheet, the GCM and RCM model simulations produce a cold and dry climate in line with the ice-sheet configuration. In southern Europe, the RCM results show that snow accumulates throughout the simulation in parts of the Alps, indicating that glaciers in that area would grow under the simulated LGM conditions.

The larger variability in LGM compared to the recent past is inherited from the global simulation and associated with variations in the North Atlantic sea ice cover (Brandefelt and Otto-Bliesner, 2009). If proxy methods for estimating palaeo temperatures are sensitive to interannual variability or extremely cold conditions our results suggests that such temperature estimates may not necessarily be representative for LGM conditions, or would at least require careful interpretation. Given the decadal variability for the North Atlantic and European sector in 1000 yr of the CCSM3 simulation, we conclude that the 50-yr period chosen for downscaling is a good representative for the whole 1000-yr simulation. Choosing another 50-yr period would not have resulted in significantly different results. This does not hold for shorter time periods. These results imply that future studies of the LGM climate in Europe should take into account long-time periods of several decades to include interannual and interdecadal variability.

Although the RCA3 results for Europe are to a large degree governed by the boundary conditions from CCSM3, the high resolution gives a more detailed climate, especially in mountainous areas and around coast lines. In spite of this advantage, the model–proxy comparison is not significantly improved by RCA3. However, the higher resolution in RCA3 enables detailed studies of, for example vegetation, ice sheet extent, variability, precipitation and lapse rate. This can provide important information on spatial variability that is essential when comparing to studies involving detailed topographic features (e.g. Kuhlemann at al., 2008). We conclude that in order to further constrain an RCM at its high level of detail, including seasonal and horizontal variability, there is a need of more proxy data that should be associated with smaller error bars than in the data used here.

Other processes influencing LGM climate that are not included in this study (e.g. dynamical ice, and atmospheric dust loads more in line with reconstructions than what is used here) could be investigated further. Such studies would also benefit from more certain proxy data, because the effect of such changes in the model is probably small compared to the present uncertainties in the proxy data.

6. Acknowledgments

This research was financed by the Swedish Nuclear Waste Commission (SKB). All model simulations with the GCM and RCM were performed on the climate computing resource Tornado funded with a grant from the Knut and Alice Wallenberg foundation. This research uses data provided by the Community Climate System Model project supported by the Directorate for Geosciences of the National Science Foundation and the Office of Biological and Environmental Research of the U.S. Department of Energy. Robert Allen, Joël Guiot, Antje Voelker, Claire Waelbroeck and Haibin Wu all kindly provided proxy data. The authors are grateful for most valuable input and comments from Barbara Wohlfarth and Jens-Ove Näslund. The authors thank two anonymous reviewers, whose comments helped to improve the text.

References

Allen, R., Siegert, M. J. and Payne, A. J. 2008. Reconstructing glacier-based climates of LGM Europe and Russia – Part 2: A dataset of LGM precipitation/temperature relations derived from degree-day modelling of palaeo glaciers. *Clim. Past.* **4**, 249–263.

Braconnot, P., Otto-Bliesner, B., Harrison, S., Joussaume, S., Peterchmitt, J.-Y. and co-authors. 2007. Results of PMIP2 coupled simulations of the Mid-Holocene and Last Glacial Maximum. Part 1: Experiments and large-scale features. *Clim. Past.* **3**, 261–277.

Brandefelt, J. and Otto-Bliesner, B. 2009. Equilibration and variability in a Last Glacial Maximum Climate simulation with CCSM3. *Geophys. Res. Lett.* **36**, L19712. doi: 10.1029/2009GL040364.

CLIMAP. 1981. Seasonal reconstructions of the Earth's surface at the last glacial maximum. In: *Map Chart Series MC-36*. Geological Society of America, Boulder, Colorado.

Collins, W. D., Bitz, C. M., Blackmon, M. L., Bonan, G. B., Bretherton, C. S. and co-authors. 2006. The Community Climate System Model (CCSM3). *J. Climate* **19**, 2122–2143.

Cramer, W., Bondeau, A., Woodward, F. I., Prentice, I. C., Betts, R. A. and co-authors. 2001. Global response of terrestrial ecosystem structure and function to CO_2 and climate change: results from six dynamic global vegetation models. *Global Change Biol.* **7**, 357–373.

Gritti, E. S., Smith, B. and Sykes, M. T. 2006. Vulnerability of Mediterranean basin ecosystems to climate change and invasion by exotic plant species. *J. Biogeogr.* **33**, 145–157.

Harrison, S. P. and Prentice, I. C., 2003. Climate and CO_2 controls on global vegetation distribution at the last glacial maximum: analysis based on palaeovegetation data, biome modelling and palaeoclimate simulations. *Global Change Biol.* **9**, 983–1004.

Hickler, T., Smith, B., Sykes, M. T., Davis, M. B., Sugita, S. and co-authors. 2004. Using a generalized vegetation model to simulate vegetation dynamics in the western Great Lakes region, USA, under alternative disturbance regimes. *Ecology* **85**, 519–530.

IPCC. 2001. Climate Change 2001: The Scientific Basis. In: *Contribution of Working Group I to the Third Assessment Report of the Intergovernmental Panel on Climate Change* (eds J.T. Houghton, Y. Ding, D.J. Griggs, M. Noguer, P.J. van der Linden and co-authors). Cambridge University Press, Cambridge, UK and New York, NY, USA, 881.

Jahn, A., Claussen, M., Ganopolski, A. and Brovkin, V. 2005. Quantifying the effect of vegetation dynamics on the climate of the Last Glacial Maximum. *Clim. Past.* **1**, 1–7.

Jansen, E., Overpeck, J., Briffa, K. R., Duplessy, J.-C. Joos, F. and co-authors. 2007. Palaeoclimate. In: *Climate Change 2007: The Physical Science Basis. Contribution of Working Group I to the Fourth Assessment Report of the Intergovernmental Panel on Climate Change* (eds S. Solomon, D. Qin, M. Manning, Z. Chen, M. Marquis and co-authors). Cambridge University Press, Cambridge, UK and New York, NY, USA.

Jones, C. G., Ullerstig, A., Willén, U. and Hansson, U. 2004. The Rossby Centre regional atmospheric climate model (RCA). Part I: Model climatology and performance characteristics for present climate over Europe. *Ambio* **33**, 199–210.

Jost, A., Lunt, D., Kageyama, M., Abe-Ouchi, A., Peyron, O. and co-authors. 2005. High-resolution simulations of the last glacial maximum climate over Europe: a solution to discrepancies with continental palaeoclimatic reconstructions? *Clim. Dyn.* **24**, 577–590.

Joussaume, S. and Taylor, K. E. 1995. Status of the Paleoclimate Modeling Intercomparison Project (PMIP). In: *Proceedings of the 1st International AMIP Science Conference* (ed. W.L. Gates). Monterrey, California, USA, 15–19 May 1995, 25–430, WCRP-92.

Kageyama, M., Lainé, A., Abe-Ouchi, A., Braconnot, P., Cortijo, E. and co-authors. 2006. Last Glacial Maximum temperatures over the North Atlantic, Europe and western Siberia: a comparison between PMIP models, MARGO sea-surface temperatures and pollen-based reconstructions. *Quat. Sci. Rev.* **25**, 2082–2102.

Kaplan, J.O., Bigelow, N.H., Prentice, I.C., Harrison, S.P., Bartlein, P.J. and co-authors. 2003. Climate change and Arctic ecosystems. 2. Modeling, paleodata-model comparisons, and future projections. *J. Geophys. Res.* **108**, 8171–8187.

Kim, S.-J., Crowley, T. J., Erickson, D. J., Govindasamy, B., Duffy, P. B. and co-authors. 2008. High-resolution climate simulation of the last glacial maximum. *Clim. Dyn.* **31**, 1–16.

Kjellström, E., Bärring, L., Gollvik, S., Hansson, U., Jones, C. and co-authors. 2005. A 140-yr simulation of European climate with the new version of the Rossby Centre regional atmospheric climate model (RCA3). In: *Reports Meteorology and Climatology*. Volume 108, SMHI, SE-60176 Norrköping, Sweden, 54.

Kjellström, E., Brandefelt, J., Näslund, J.O., Smith, B., Strandberg, G. and co-authors. 2009. Climate conditions in Sweden in a 100,000 yr time perspective. *Svensk Kärnbränslehantering AB, report TR-09–04*, 139.

Kjellström, E., Brandefelt, J., Näslund, J.O., Smith, B., Strandberg, G. and co-authors. 2010. Simulated climate conditions in Fennoscandia during a MIS 3 stadial. *Boreas* **10**, doi: 10.1111/j.1502-3885.2010.00143.x.

Kjellström, E., Nikulin, G., Hansson, U., Strandberg, G. and Ullerstig, A. 2011. 21st century changes in the European climate: uncertainties derived from an ensemble of regional climate model simulations. *Tellus* **63A**, 24–40.

Koca, D., Smith, B. and Sykes, M. T. 2006. Modelling regional climate change effects on Swedish ecosystems. *Clim. Change* **78**, 381–406.

Kuhlemann, J., Rohling, E.J., Krumrei, I., Kubik, P., Ivy-Ochs, S. and co-authors. 2008. Regional synthesis of Mediterranean atmospheric circulation during the Last Glacial Maximum. *Science*, **321**, 1338–1340.

Laîné, H., Kageyama, M., Salas-Mélia, D., Voldoire, A., Rivière, G. and co-authors. 2009. Northern hemisphere storm tracks during the last glacial maximum in the PMIP2 ocean-atmosphere coupled models: energetic study, seasonal cycle, precipitation. *Clim. Dyn.*, **32**, 593–614, doi: 10.1007/s00382-008-0391-9.

Lambeck, K. 2004. Sea-level change through the last glacial cycle: geophysical, glaciological and palaeogeographic consequences. *Comptes Rendus Geoscience* **336**, 677–689.

MARGO Project Members. 2009. Constraints on the magnitude and patterns of ocean cooling at the Last Glacial Maximum. *Nat. Geosci.* **2**, doi: 10.1038/NGEO411.

Mahowald, N. M., Yoshioka, M., Collins, W. D., Conley, A. J., Fillmore, D. W. and co-authors. 2006. Climate response and radiative forcing from mineral aerosols during the last glacial maximum, pre-industrial, current and doubled-carbon dioxide climates. *Geophys. Res. Lett.* **33**, L20705, doi: 10.1029/2006GL026126.

Mangerud, J., Gosse, J., Matiouchkov, A. and Dolvik, T. 2008. Glaciers in the polar Urals, Russia, were not much larger during the last global glacial maximum than today. *Quat. Sci. Rev.* **27**, 1047–1057.

Miller, P. A., Giesecke, T., Hickler, T., Bradshaw, R. H. W., Smith, B. and co-authors. 2008. Exploring climatic and biotic controls on Holocene vegetation change in Fennoscandia. *J. Ecol.* **96**, 247–259.

Moberg, A., Gouirand, I., Wohlfarth, B., Schoning, K., Kjellström, E. and co-authors. 2006. Climate in Sweden during the past millennium—evidence from proxy data, instrumental data and model simulations. *Report TR-06–35, Svensk Kärnbränslehantering AB*, 87.

Morales, P., Sykes, M. T., Prentice, I. C., Smith, P., Smith, B. and co-authors. 2005. Comparing and evaluating process-based ecosystem model predictions of carbon and water fluxes in major European forest biomes. *Global Change Biol.* **11**, 2211–2233.

Morales, P., Hickler, T., Rowell, D. P., Smith, B. and Sykes, M. T. 2007. Changes in European ecosystem productivity and carbon balance driven by Regional Climate Model output. *Global Change Biol.* **13**, 108–122.

Otto-Bliesner, B. L., Thomas, R., Brady, E. C., Ammann, C., Kothavala, Z. and co-authors. 2006a. Climate sensitivity of moderate and low-resolution versions of CCSM3 to pre-industrial forcings. *J. Climate* **19**, 2567–2583.

Otto-Bliesner, B. L., Brady, E. C., Clauzet, G., Thomas, R., Levis, S. and co-authors. 2006b. Last glacial maximum and Holocene climate in CCSM3. *J. Climate* **19**, 2526–2544.

Otto-Bliesner, B. L., Hewitt, C. D., Marchitto, T. M., Brady, E., Abe-Ouchi, A. and co-authors. 2007. Last Glacial Maximum ocean thermohaline circulation: PMIP2 model intercomparisons and data constraints. *Geophys. Res. Lett.* **34**, L12706.

Otto-Bliesner, B. L., Schneider, R., Brady, E. C., Kucera, M., Abe-Ouchi, A. and co-authors. 2009. A comparison of PMIP2 model simulations and the MARGO proxy reconstruction for tropical sea surface temperatures at last glacial maximum. *Clim. Dyn.* **32**, 799–815, doi: 10.1007/s00382-008-0509-0.

Peltier, W. R. 1994. Ice age paleotopography. *Science* **265**, 195–201.

Peltier, W. R. 2004. Global glacial isostasy and the surface of the ice-age circulation. Earth: The ICE-5G (VM2) model and GRACE, Annual Review of Earth Planet. *Sciences* **32**, 111–149.

Pollard, D. and Barron, E. J. 2003: Causes of model-data discrepancies in European climate during oxygen isotope stage 3 with insights from the last glacial maximum. *Quat. Res.* **59**, 108–113.

Räisänen, J., Hansson, U., Ullerstig, A., Döscher, R., Graham, L. P. and co-authors. 2003. GCM driven simulations of recent and future climate with the Rossby Centre coupled atmosphere—Baltic Sea regional climate model RCAO. In: *Reports Meteorology and Climatology*. Volume 101, Swedish Meteorological and Hydrological Institute, SE-601 76 Norrköping, Sweden, 61.

Räisänen, J., Hansson, U., Ullerstig, A., Döscher, R., Graham, L. P. and co-authors. 2004. European climate in the late twenty-first century: regional simulations with two driving global models and two forcing scenarios. *Clim. Dyn.* **22**, 13–31.

Ramstein, G., Kageyama, M., Guiot, J., Wu, H., Hély, C. and co-authors. 2007. How cold was Europe at the Last Glacial Maximum? A synthesis of the progress achieved since the first PMIP model-data comparison. *Clim. Past*. **3**, 331–339.

Randall, D. A., Wood, R. A., Bony, S., Colman, R., Fichefet, T. and co-authors. 2007. Climate models and their evaluation. In: *Climate Change 2007: The Physical Science Basis. Contribution of Working Group I to the Fourth Assessment Report of the Intergovernmental Panel on Climate Change* (eds S. Solomon, D. Qin, M. Manning, Z. Chen, M. Marquis and co-authors). Cambridge University Press, Cambridge, UK and New York, NY, USA.

Ray, N. and Adams, J. M. 2001. A GIS-based Vegetation Map of the World at the Last Glacial Maximum (25,000–15,000 BP). Internet Archaeology 11. Available at: http://intarch.ac.uk/journal/issue11/rayadams_toc.html. Accessed 24 Sep 2010.

Renssen, H. and Vandenberghe, J. 2003. Investigation of the relationship between permafrost distribution in NW Europe and extensive winter sea-ice cover in the North Atlantic Ocean during the cold phases of the Last Glaciation. *Quat. Sci. Rev.* **22**, 209–233.

Roche, D. M., Dokken, T. M., Goosse, H., Renssen, H. and Weber, S. L. 2006. Climate of the last glacial maximum: sensitivity studies and model-data comparison with the LOVECLIM coupled model. *Clim. Past. Discuss.* **2**, 1105–1153.

Rummukainen, M. 2010. State-of-the-art with regional climate models. *Wiley Interdisciplinary Rev.: Clim. Change*, **1**, 82–96, doi: 10.1002/wcc.8

Rummukainen, M., Räisänen, J., Ullerstig, A., Bringfelt, B., Hansson, U. and co-authors. 1998. RCA—Rossby Centre regional Atmospheric climate model: model description and results from the first multi-year simulation. In: *Reports Meteorology and Climatology*. Volume 83, Swedish Meteorological and Hydrological Institute, SE-601 76 Norrköping, Sweden, 76.

Rummukainen, M., Räisänen, J., Bringfelt, B., Ullerstig, A., Omstedt, A. and co-authors. 2001. A regional climate model for northern Europe: model description and results from the downscaling of two GCM control simulations. *Clim. Dyn.* **17**, 339–359.

Samuelsson, P., Jones, C., Willén, U., Gollvik, S., Hansson, U. and co-authors. 2011. The Rossby Centre Regional Climate Model RCA3: Model description and performance. *Tellus* **63A**, 4–23.

Sarnthein, M., Pflaumann, U. and Weinelt, M. 2003. Past extent of sea ice in the northern North Atlantic inferred from foraminiferal paleotemperature estimates. *Paleoceanography* **18**(2), 1047, doi: 10.1029/2002PA000771.

Schneider von Deimling, T., Ganopolski, A., Held, H. and Rahmstorf, S., 2006. How cold was the Last Glacial Maximum. *Geophys. Res. Lett.*, **33**, L14709, doi: 10.1029/2006GL026484.

Sitch, S., Smith, B., Prentice, I. C., Arneth, A., Bondeau, A. and co-authors. 2003. Evaluation of ecosystem dynamics, plant geography and terrestrial carbon cycling in the LPJ Dynamic Global Vegetation Model. *Global Change Biol.* **9**, 161–185.

Sitch, S., Brovkin, V., von Bloh, W., van Vuuren, D., Eickhout, B. and co-authors. 2005. Impacts of future land cover changes on atmospheric CO_2 and climate. *Global Biogeochem. Cycles* **19**, GB2013–2027.

Sitch, S., Huntingford, C., Gedney, N., Levy, P. E., Lomas, M. and co-authors. 2008. Evaluation of the terrestrial carbon cycle, future plant geography and climate-carbon cycle feedbacks using five Dynamic Global Vegetation Models (DGVMs). *Global Change Biol.* **14**, 2015–2039.

Smith, B., Prentice, I. C. and Sykes, M. T. 2001. Representation of vegetation dynamics in modelling of terrestrial ecosystems: comparing two contrasting approaches within European climate space. *Global Ecol. Biogeogr.* **10**, 621–637.

Smith, B., Knorr, W., Widlowski, J. L., Pinty, B. and Gobron, N. 2008. Combining remote sensing data with process modelling to monitor boreal conifer forest carbon balances. *Forest Ecol. Manage.* **255**, 3985–3994.

Smith, B., Samuelsson, P., Wramneby, A. and Rummukainen, R. 2011. A model of the coupled dynamics of climate, vegetation and ecosystem biogeochemistry for regional applications. *Tellus* **63A**, 87–106.

Weber, S. L., Drijfhout, S. S., Abe-Ouchi, A., Crucifix, M., Eby, M. and co-authors. 2007. The modern and glacial overturning circulation in the Atlantic ocean in PMIP coupled model simulations. *Clim. Past*. **3**, 51–64.

Wolf, A., Callaghan, T. V. and Larson, K. 2008. Future changes in vegetation and ecosystem function of the Barents Region. *Clim. Change* **87**, 51–73.

Woodward, F. I. and Williams, B. G., 1987. Climate and plant distribution at global and local scales. *Vegetation* **69**, 189–197.

Wu, H., Guiot, J., Brewer, S. and Guo, Z. 2007. Climatic changes in Eurasia and Africa at the last glacial maximum and mid-Holocene: reconstruction from pollen data using inverse vegetation modeling. *Clim. Dyn.* **29**, 211–229.

Wramneby, A., Smith, B., Zaehle, S. and Sykes, M. T. 2008. Parameter uncertainties in the modelling of vegetation dynamics—effects on tree community structure and ecosystem functioning in European forest biomes. *Ecol. Model.* **216**, 277–290.

Yurova, A. Y. and Lankreijer, H. 2007. Carbon storage in the organic layers of boreal forest soils under various moisture conditions: a model study for Northern Sweden sites. *Ecol. Model.* **204**, 475–484.

Zaehle, S., Sitch, S., Prentice, I. C., Liski, J., Cramer, W. and co-authors. 2006. The importance of representing age-related decline in forest NPP for modeling regional carbon balances. *Ecol. Appl.* **16**, 1555–1574.